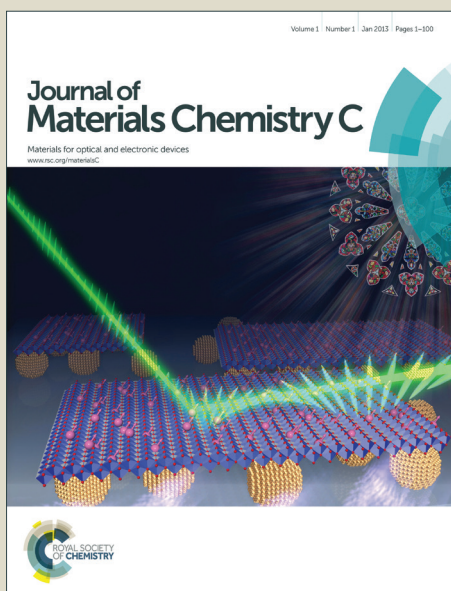


Journal of Materials Chemistry C

Accepted Manuscript



This is an *Accepted Manuscript*, which has been through the Royal Society of Chemistry peer review process and has been accepted for publication.

Accepted Manuscripts are published online shortly after acceptance, before technical editing, formatting and proof reading. Using this free service, authors can make their results available to the community, in citable form, before we publish the edited article. We will replace this *Accepted Manuscript* with the edited and formatted *Advance Article* as soon as it is available.

You can find more information about *Accepted Manuscripts* in the [Information for Authors](#).

Please note that technical editing may introduce minor changes to the text and/or graphics, which may alter content. The journal's standard [Terms & Conditions](#) and the [Ethical guidelines](#) still apply. In no event shall the Royal Society of Chemistry be held responsible for any errors or omissions in this *Accepted Manuscript* or any consequences arising from the use of any information it contains.

High Efficiency Non-Dopant Blue Organic Light-Emitting Diodes Based on Anthracene-Based Fluorophores with Molecular Design of Charge Transport and Red-Shifted Emission Proof

Cheng-Lung Wu,^{ab} Che-Hong Chang,^{ac} Yung-Ting Chang,^a Chin-Ti Chen,^{*a} Chao-Tsen Chen,^{*b} Chi-Jung Su,^{*c}

Received (in XXX, XXX) Xth XXXXXXXXX 20XX, Accepted Xth XXXXXXXXX 20XX

DOI: 10.1039/b000000x

A new series of 9,10-diphenylanthracene (DPA)-based blue fluorophores have been synthesized and characterized for OLED applications. These fluorophores have bulky substituent on C-2 position, such as triphenylsilane of **TPSDPA** and mesitylene of **TMPDPA**. C-2 substituent also includes electron transport diphenylphosphine oxide of **PPODPA** and dimesitylene borane of **BMTDPA**, or hole transport of *N*-phenyl-naphthalen-1-amine of **NPADPA**. For **TMPDPA** blue fluorophores, 9,10-diphenyl substituents of the anthracene core are further attached with hole-transporting 9*H*-carbazole (**CBZDPA**) and electron-transporting 2-phenyl-1,3,4-oxadiazole (**OXDDPA**). Absorption and emission spectroscopic properties of all DPA-derived fluorophores, either in solution or in condensed phase, were fully characterized and HOMO/LUMO energy levels of these fluorophores were determined. The frontier molecular orbitals of these DPA derivatives were analysed by theoretical methods in gauging the possible intramolecular charge transfer (ICT) characteristic. Whereas the blue emission is best preserved in **TMPDPA**, of which non-conjugated and bulky mesitylene group suppresses emission from red shifting, ICT is attributed to the deteriorate emission of **NPADPA** and **BMTDPA**. In solid state, **PPODPA** suffered from red-shifted and weakening emission due to the adverse crystallization, which is promoted by the dipolar nature of diphenylphosphine oxide substituent. Non-dopant OLEDs were fabricated with **DPA**, **TPSDPA**, **TMPDPA**, **PPODPA**, **CBZDPA** and **OXDDPA**, respectively. Compared with that of **DPA** OLED, except for **PPODPA**, electroluminescence efficiency of these DPA derivatives was found significantly improved. Particularly, **CBZDPA** and **OXDDPA** OLEDs exhibited the best external quantum efficiency of 4.5 and 4.0 % with true blue colour, CIE_{x,y} (0.17, 0.17) and CIE_{x,y} (0.16, 0.18), respectively. Improved electroluminescence efficiency can be attributed to the molecular charge transport design of **CBZDPA** and **OXDDPA**.

Introduction

Organic light-emitting diodes (OLEDs) remain a subject of intense investigation because of their potential applications in high-quality flat-panel displays and solid state lighting, with some consumer devices such as cell phones and digital cameras incorporating OLED screens already available in the market. OLEDs for full colours displays are showing great promise, and are required for red, green and blue-emitting materials. However, highly efficient true-blue (a Commission Internationale de l'Eclairage, CIE_{x,y} coordinate of $y < 0.20$) phosphorescent emitters are still relatively rare. More critically, there is still rare true-blue phosphorescent emitter with high photoluminescent quantum efficiency that is stable enough for practical

^aInstitute of Chemistry, Academia Sinica, Taipei 11529, Taiwan
E-mail: chintchen@gate.sinica.edu.tw; FAX: +886 2 27831237;
Tel: +886 2 27898542

^bDepartment of Chemistry, National Taiwan University, Taipei 10617, Taiwan

^cSchool of Medical Applied Chemistry, Chung Shan Medical University, Taichung 40201, Taiwan

applications.¹⁻⁵ Therefore, blue electrofluorescence materials have been revived and become highly demanded by the energy-saving solid-state lighting (SSL) utilizing hybrid white OLED.⁶⁻⁹ Anthracene has been intensively used as an attractive building block and starting material for blue fluorescence OLEDs,¹⁰⁻⁶⁰ since its derivatives usually have high fluorescence quantum yield and wide energy band-gap in solution. However, the planarity of anthracene molecular structure is prone to aggregate in solid state, which causes fluorescence quenching and emission wavelength red-shifting. For examples, two perpendicular phenyl substituents at C-9 and C-10 positions of 9,10-diphenylanthracene (DPA) cannot completely overcome the fluorescence quenching and red-shifting problems through steric hindrance approach.¹⁰ The bulky substituent at C-2 position of DPA can further prevent the molecule from aggregation and hence improve the performance of OLED further.^{13,14} However, red-shifted emission is still observed in many cases of 2-substituted DPA derivatives.

In this paper, in order to reduce the emission red-shifting in solution as well as in solid state, we have synthesized and systematically examined a series of chemical functionality with

sterical hindrance at C-2 position of DPA. We have mesitylene, triphenylsilane, diphenylphosphine oxide, dimesitylborane, and

N-phenylnaphthalen-1-amine of **TMPDPA**, **TPSDPA**, **PPODPA**, **BMTDPA**, and **NPADPA**, respectively (Figure 1).

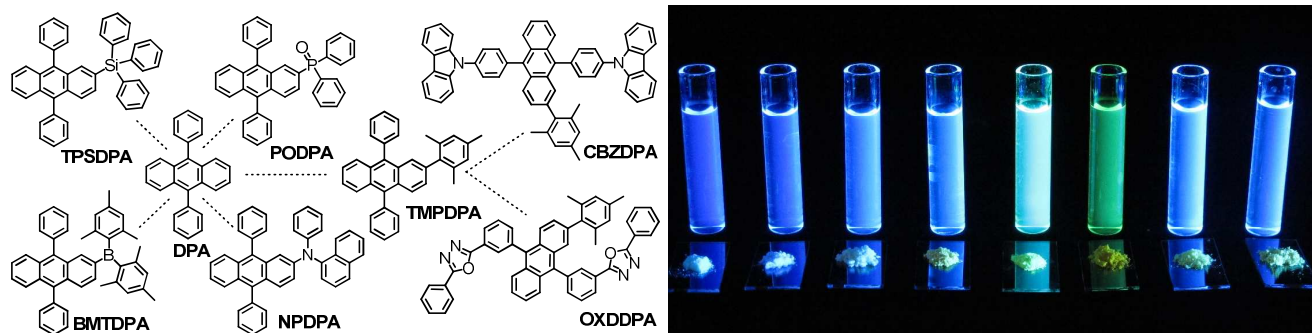


Fig. 1 Left: chemical structure of DPA derivatives. Right: solution (dichloromethane) and solid state fluorescence image of **DPA**, **TMPDPA**, **TPSDPA**, **PPODPA**, **BMTDPA**, **NPADPA**, **CBZDPA**, **OXDDPA** from left to right, respectively.

Moreover, by introducing charge transporting moiety, either 9*H*-carbazole or 2-phenyl-1,3,4-oxadiazole, on the phenyl substituent at C-9 and C-10 positions of **TMPDPA**, the performance of OLEDs based on either **CBZDPA** or **OXDDPA** was found significantly improved in terms of electroluminescence (EL) efficiency with little compromise of blue colour purity (Fig. 1).

of materials by gradient sublimation is necessary prior to device fabrication. All of these DPA derivatives were fully characterized by ¹H and ¹³C NMR and mass spectrometry and they were consistent with the proposed chemical structures.

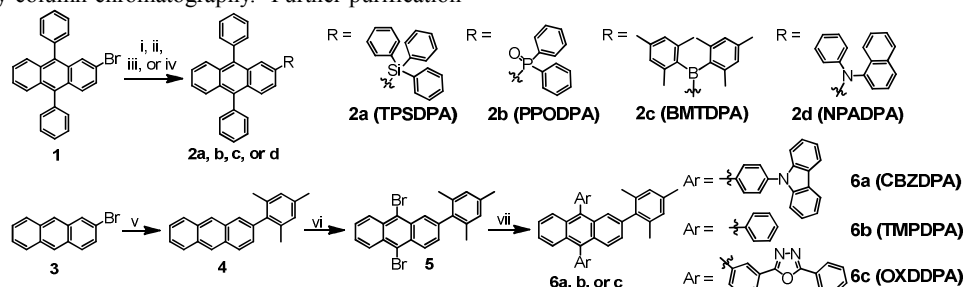
Thermal Properties

The thermal properties of these DPA derivatives were characterized by using thermogravimetric analysis (TGA) and differential scanning calorimetry (DSC). All key data were shown in Fig. 2 and Table 1. **TMPDPA**, **TPSDPA**, **PPODPA**, **BMTDPA** and **NPADPA**, C-2 modified DPA derivatives, exhibited high decomposition temperatures (*T_d*, corresponding to 5% weight loss) of 332, 361, 398, 378, and 335 °C, respectively. Moreover, **CBZDPA** and **OXDDPA** have a even higher decomposition temperatures, 416 and 449 °C, respectively. Based on the high *T_d*, all these DPA derivatives are capable of enduring vacuum thermal deposition process in OLED fabrication. Among these DPA derivatives including parent **DPA**, distinct exothermic signal of crystallization temperature (*T_c*) was identified only for **DPA**, **TPSDPA**, and **PPODPA**. Only **PPODPA** of these three compounds possesses bipolar characteristic due to the electron deficient diphenylphosphine oxide. The crystallization feature of the bipolar material is particularly unflavoured for light-emitting in OLED application.

Results and discussion

Synthesis

As shown in Scheme 1, 2-bromo-9,10-diphenylanthracene (**1**) was lithiated with *n*-butyllithium at -78 °C, followed by the reaction of different electrophile to afford **TPSDPA** (**2a**), **PPODPA** (**2b**), and **BMTDPA** (**2c**). Differently, **NPADPA** (**2d**) was obtained from **1** via Pd-catalyzed amination with *N*-phenylnaphthalen-1-amine. **CBZDPA** (**6a**), **TMPDPA** (**6b**), and **OXDDPA** (**6c**) were synthesized through a three-step procedure. First, 2-bromoanthracene (**3**) was coupled to 2,4,6-trimethylboronic acid via Suzuki-Miyaura coupling reaction to afford 2-(1,3,5-trimethylphenyl)anthracene (**4**). Second, compound **4** was brominated at C-9 and C-10 positions by NBS. Third, the resulting 9,10-dibromo-2-(1,3,5-trimethylphenyl)anthracene (**5**) was converted to desired **6a**, **6b**, or **6c** via Suzuki-Miyaura coupling reaction with pre-synthesized boronic ester or boronic acid. The compounds were readily purified by column chromatography. Further purification



Scheme 1 Reagents and conditions: i) (a) *n*BuLi, ether, -78 °C, 45 min, (b) chlorotriphenylsilane, -78 °C → rt, 12 hr, ii) (a) *n*-BuLi, ether, -78 °C, 45 min, (b) chlorodiphenylphosphine, -78 °C → rt, 12 hr, (c) H₂O₂, 12 hr, iii) (a) *n*-BuLi, THF, -78 °C, 45 min, (b) dimesitylboron fluoride, -78 °C → rt, 12 hr, iv) *N*-phenylnaphthalen-1-amine, NaOtBu, P(*t*-Bu)₃, Pd(OAc)₂, xylene, 120 °C, 16 hr, v) 2,4,6-trimethylphenylboronic acid, cat. Pd(PPh₃)₄, 2 M K₂CO_{3(aq)}, ethanol, toluene, 80 °C, 12 hr, vi) NBS, CHCl₃, 50 °C, 2 hr, vii) phenylboronic acid or pinacolborane derivative of 9-phenyl-9*H*-carbazole or 2,5-diphenyl-1,3,4-oxadiazole, cat. Pd(PPh₃)₄, 2 M K₂CO_{3(aq)}, ethanol, toluene, 80 °C, 12 hr.

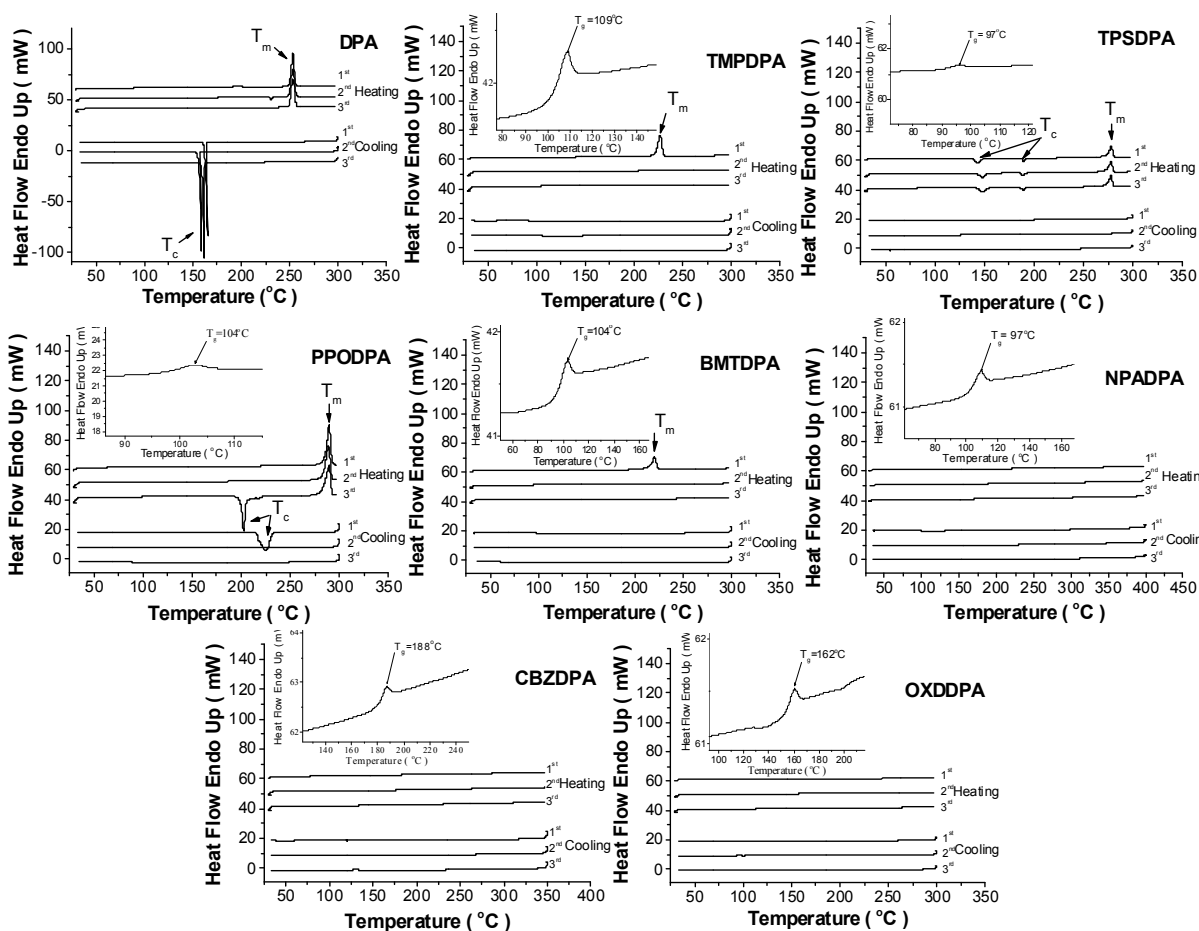


Fig. 2 DSC thermograms of DPA, TMPDPA, TPSDPA, PPODPA, BMTDPA, NPADPA, CBZDPA and OXDDPA.

The T_g values of **CBZDPA** and **OXDDPA** were 188 and 162 °C, which were much higher than other derivatives (T_g around 97~109 °C). In addition to **NPADPA**, **CBZDPA** and **OXDDPA** are the only two DPA derivatives without being detected (less than 350~400 °C) for both melting (T_m) and crystallization (T_c) temperatures. The superior thermal properties of **CBZDPA** and **OXDDPA** could increase the phase stability of the amorphous thin film, which is beneficial to the operation lifetime and maybe the efficiency of devices. From thermal property studies, the structural feature of **CBZDPA** and **OXDDPA** can be identified as most effective considering the application for OLEDs.

Absorption and Emission Spectroscopic Characterization

The absorption and emission spectra of DPA derivatives were studied in various solvents (toluene, dichloromethane, DMF, and THF) as well as in the solid thin film, which was prepared by spin-coating dichloromethane solution on quartz plates. As shown in Fig. 3, parent compound **DPA** exhibits broadening and red-shifting spectra of absorption and emission in solid state, when compared with those in solution. Its solid state Φ_f is ~60%, which is reasonable good but significantly decreases from ~90% in solution. This is very common for planar polycyclic aromatic hydrocarbons (PAHs) such as **DPA**. Spectroscopic feature

(including those vibronic structures) observed for **DPA** is attributed to the $\pi\pi^*$ electronic transition, of which corresponding energy is sensitive to the molecular interaction ($\pi\pi$ molecular stacking) in condense phase.

Among C-2 modified DPA derivatives, such broadening and red-shifting spectroscopic feature is significantly suppressed especially in the case of **TMPDPA**. Based on the present study, sterically hindered mesityl group on C-2 position is a very effective structural factor for preserving the deep blue fluorescence color of DPA derivatives in solid state. C-2 modified DPA derivatives, **TPSDPA**, **PPODPA**, **BMTDPA**, and **NPADPA**, are designed along the line. However, significantly red-shifted spectra of both absorption and emission take place and it is detrimental to the blue color purity, particularly for **PPODPA**, **BMTDPA**, and **NPADPA**, the most serious three. Based on our spectroscopic observation, we deduce that the broadening and red-shifting spectroscopic features of these DPA derivatives are caused by various reasons.

We did not expect that triphenylsilyl group is not as effective as mesityl group in preventing spectra of **DPA** from broadening or red-shifting in solid state. However, we notice that both solution $\lambda_{\max}^{\text{ab}}$ and $\lambda_{\max}^{\text{fl}}$ of **TPSDPA** are substantially longer than those of **TMPDPA**, of which $\lambda_{\max}^{\text{ab}}$ and $\lambda_{\max}^{\text{fl}}$ are only slightly longer than those of **DPA** (Table 1). The more red-shifted

spectra observed for **TPSDPA** than **TMPDPA** can be ascribed to the σ -conjugation of silyl group. In solid state, molecular packing of **TPSDPA** probably intensifies such σ -conjugation and further red-shifts the emission spectra. However, such molecular packing slightly impairs its solid state Φ_f . It remains as high as $\sim 70\%$, moderately less than 86% in solution. In terms of Φ_f , **TPSDPA** is rather different from **TMPDPA**, of which fluorescence is significantly quenched in solid state showing solid state Φ_f only $\sim 40\%$, much smaller than 90% in solution. Within the context, we think the especially pronounced red-shifting thin film or powder emission spectra of **PPODPA** may be also explained by molecular packing, since its solution $\lambda_{\max}^{\text{em}}$ is

relatively short in wavelength ($448\text{--}452\text{ nm}$ vs. 487 nm in solid state). In addition, the molecular packing of **PPODPA** may be the adverse factor that more or less jeopardizes its solid state $\Phi_f \sim 30\%$, which is significantly lower than solution $\Phi_f \sim 83\%$ (Table 1). Potentially, there is excimer formation from the molecular packing of **PPODPA**. Such solid state properties make **PPODPA** an unfavorable blue light-emitting material in OLEDs.

On the other hand, relatively long wavelength of solution $\lambda_{\max}^{\text{em}}$ observed for both **BMTDPA** and **NPADPA** should be attributed to the electronic effect of the π -donor of *N*-phenyl naphthalen-1-amine and the π -acceptor of dimesitylborane, respectively.

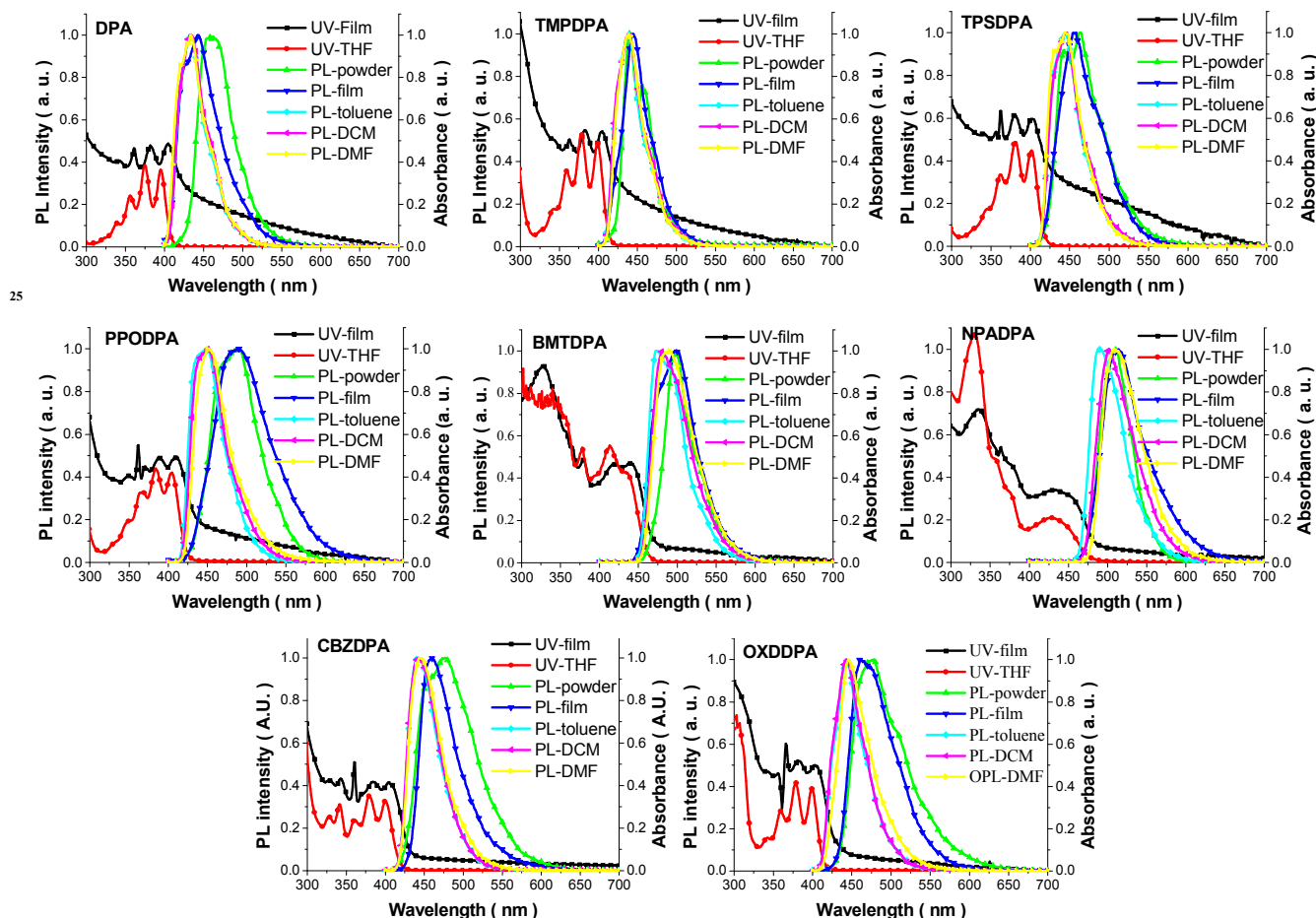


Fig. 3 The absorption and photoluminescence (PL) spectra of **DPA** and **DPA** derivatives in solution and in condensed phase.

In other words, intramolecular charge transfer (ICT), which is lower in energy compared with that of $\pi\pi^*$, contributes to the electronic transition process. Less well resolved vibronic bands observed in the absorption spectra (Fig. 3) of **BMTDPA** and **NPADPA** is consistent with our inference. In addition, **BMTDPA** and **NPADPA** are two **DPA** derivatives showing the most distinct trend of fluorescence solvatochromism (Table 1), which is also consistent with the ICT feature that we propose above. Otherwise, low Φ_f and solvent dependent PL wavelength may be attributed to photoinduced electron transfer (PET), which has been observed for arylamine-substituted electron deficient fluorophores.⁶¹⁻⁶³ In fact, **NPADPA** has the lowest Φ_f of 33 and

20%, in solution and solid state, respectively, among **DPA** derivatives in present study.

Since **TMPDPA** has the least broadening and red-shifting spectra among **DPA** derivatives, we choose it for further functionalization with charge transport, i.e., hole transport of **CBZDPA** and electron transport of **OXDDPA**. Based on their well resolved vibronic band of the absorption spectra and relatively high solid state Φ_f , 60 and 70%, respectively (Fig. 3 and Table 1), we can reasonably infer that there is little ICT involved in the spectroscopy electronic transition of both **CBZDPA** and **OXDDPA**. Solution absorption $\lambda_{\max}^{\text{ab}}$ and emission $\lambda_{\max}^{\text{em}}$ of both **CBZDPA** and **OXDDPA** are nearly as

short as those of **TMPDPA** (Fig. 3 and Table 1), indicating there is limited π -conjugation between the charge transport substituent and anthracene core. Finally, based on Φ_f data both in solution and in solid state, all of DPA derivatives reported herein exhibit

5 common and typical aggregation caused quenching (ACQ) emission instead of aggregation-induced emission (AIE) or aggregation induced enhanced emission (AIEE).⁶⁴⁻⁶⁶

Table 1. Optical and thermal properties of DPA-based derivatives

DPA derivatives	Solution				Solid		T_g (°C)	T_c (°C)	T_m (°C)	T_d (°C)	LUMO/HOMO (eV) ^[f]
	$\lambda_{\text{on set}}^{\text{ab}}$	$\lambda_{\text{max}}^{\text{ab}}$, (nm) ^[a]	$\lambda_{\text{max}}^{\text{fl [b]}}$, $\lambda_{\text{max}}^{\text{fl [d]}}$ (nm)	$\lambda_{\text{max}}^{\text{fl [c]}}$	$\lambda_{\text{max}}^{\text{ab}}$, (nm)	Φ_f (%)					
DPA	375, 410	432, 433, 433	90	442	~60	[e]	165	253	315	2.84/ 5.81	
TMPDPA	378, 413	438, 438, 439	90	444	~40	109	[e]	227	332	3.04/ 5.94	
TPSDPA	380, 421	443, 446, 444	86	456	~70	97	189	277	361	2.96/ 5.93	
PPODPA	384, 420	448, 452, 450	83	487	~30	104	202	289	398	3.04/ 5.90	
BMTDPA	413, 460	473, 480, 490	61	499	~50	104	[e]	220	378	3.23/ 5.87	
NPADPA	429, 473	490, 502, 507	33	513	~20	97	[e]	[e]	335	3.20/ 5.46	
CBZDPA	379, 417	442, 442, 445	94	459	~60	188	[e]	[e]	416	3.07/ 5.94	
OXDDPA	379, 413	443, 443, 446	88	461	~70	162	[e]	[e]	449	2.86/ 5.74	

[a] in THF. [b] in toluene. [c] in dichloromethane. [d] in DMF. [e] not observed. [f] HOMO energy was determined using an AC-2 photoelectron spectrometer (Riken-Keiki AC-2); LUMO energy was determined as the lowest photo-excitation state energy from the on-set absorption energy of thin film absorption spectra.

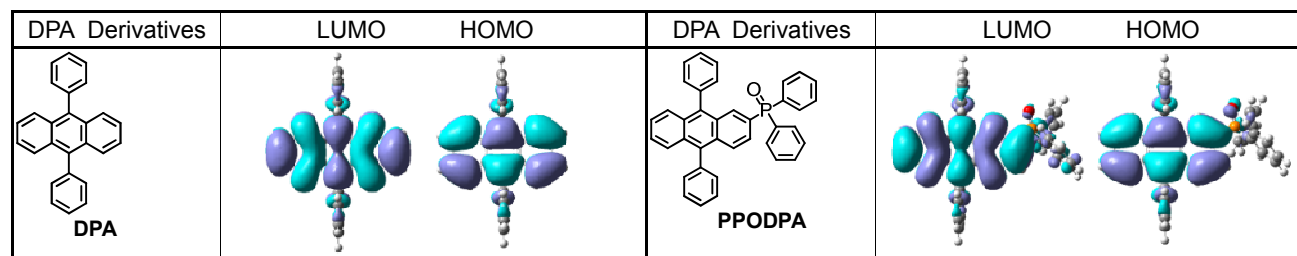
Theoretical Estimation of Frontier Molecular Orbitals

The molecular structures of **DPA**, **TPSDPA**, **TMPDPA**, **PPODPA**, **BMTDPA**, **NPADPA**, **CBZDPA**, and **OXDDPA** were optimized by applying density functional theory (DFT) with the hybrid B3LYP functional and 6-31G* basis set. With the optimized structure, calculations on the electronic ground states of these DPA derivatives were processed using DFT with the hybrid B3LYP functional and 6-31G* basis set.⁶⁷ The singlet excited states of these DPA derivatives were studied with time-dependent density functional theory (TDDFT) by using the hybrid B3LYP functional.⁶⁸ All calculations were performed with a developmental version of Q-Chem.⁶⁹ We display a comparison of the corresponding HOMO and LUMO of these DPA derivatives in S_0 state, where materials are in gas phase approximate to the solution state instead of condense phase. Because electronic excitation from the HOMO to the LUMO produces the first singlet excited state S_1 (a Franck-Condon excited state), the orbital features presented in Fig. 4 provide important clues towards understanding the nature of optical accessible first excited state.

From the contour plots of **DPA**, **TMPDPA**, **TPSDPA**, and

PPODPA, both HOMO and LUMO mainly consist of the π -conjugation of anthracene core. Similar HOMO/LUMO contour plots was found for **OXDDPA** with little π -conjugation extended into substituents on C-9 and C-10 positions. Differently, the HOMO and/or the LUMO of **BMTDPA** and **NPADPA** were found significantly extended beyond anthracene core into *N*-phenylnaphthalen-1-amine and dimesitylborane, respectively. Such theoretical findings are quite consistent with ICT feature proposed from the spectroscopic characterization in previous section.

Considering the large twist angle (dihedral angle $\sim 80^\circ$) between the phenyl ring and anthracene core, it is to our surprise that π -conjugation based on HOMO contour plots of **CBZDPA** actually expands extensively into one of the phenyloxadiazole substituents on C-9 and C-10 positions, whereas π -conjugation of LUMO is pretty much confined on the anthracene core. The implication from such theoretical results of **CBZDPA** is somewhat contradictory to spectroscopy experimental results, i.e., well resolved solution absorption vibronic bands, no clear trend of fluorescence solvatochromism, and reasonable solution Φ_f .



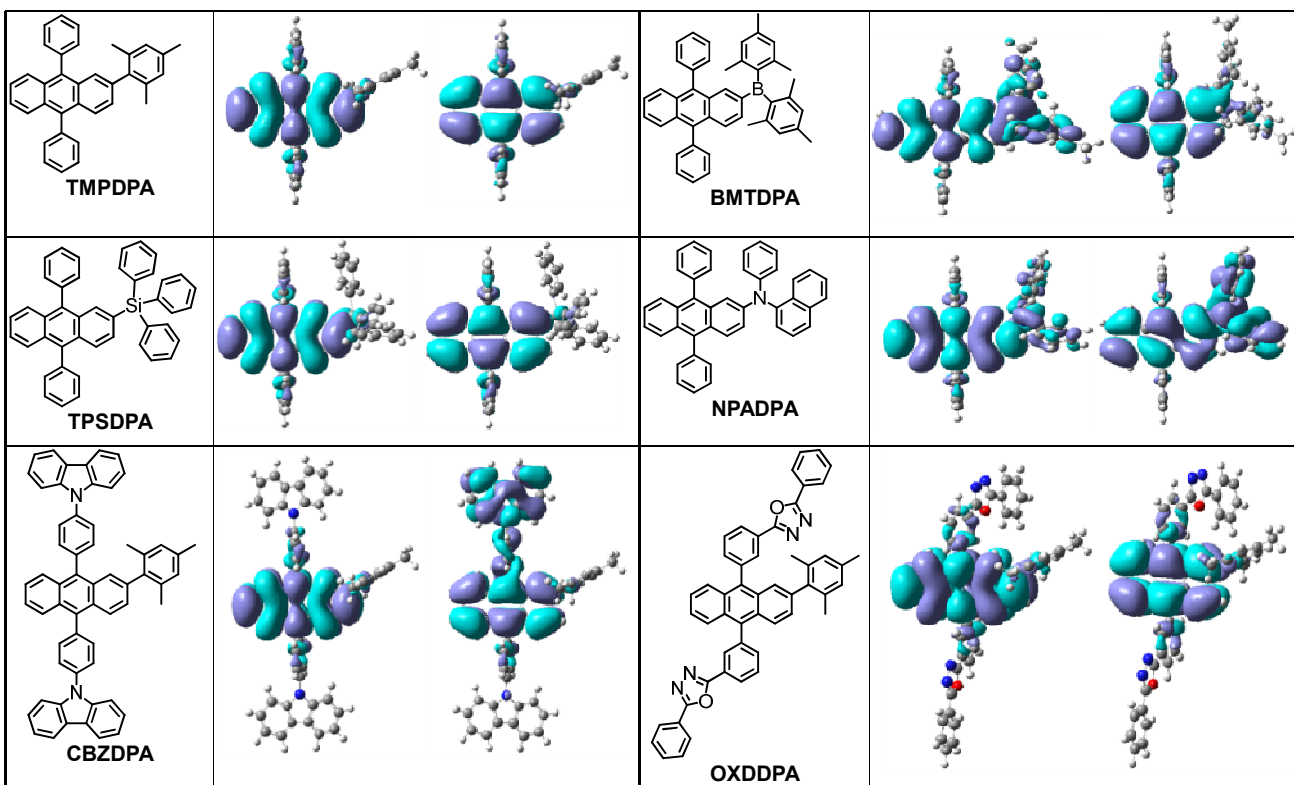


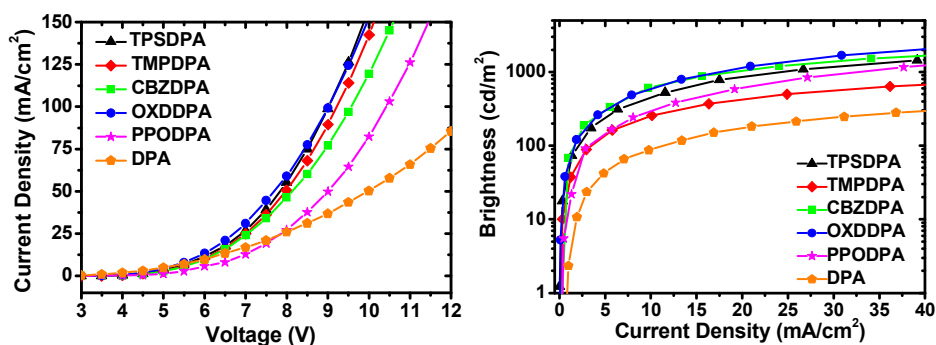
Fig. 4 Calculated spatial distributions of the HOMO and LUMO of DPA and DPA derivatives.

Characterization of OLEDs and Charge Transport

All OLEDs were fabricated by sequential thermal vacuum deposition of thin film layer of organic material and LiF/Al as the final cathode electrode on ITO (indium-tin-oxide)-coated glass substrate. Excluding the spectroscopy unsatisfied **BMTDPA** and **NPADPA**, six devices were fabricated for six blue DPA derivatives, with the device configuration of ITO/NPB(30 nm)/TCTA(10 nm)/DPAs(30 nm)/TPBI(30 nm)/LiF(1)/Al, where 4,4'-bis[*N*-(1-naphthyl)-*N*-phenyl]-biphenyl (NPB) is a common hole-transporting layer, 2,2',2''-(1,3,5-benzinetriyl)-tris(1-phenyl-1-*H*-benzimidazole) (TPBI) is a common electron-transporting layer, and LiF/Al were used as the electron injecting layer and cathode. In each device, between NPB and DPAs light-emitting layers, there is a thin layer of tris(4-carbazoyl-9-ylphenyl)amine (TCTA), which serves multi-function including hole-transporting layer, exciton blocking layer, and smoothing the alignment of HOMO energy level inside the device. Such

interlayer can decrease turn-on voltage and enhance the charge recombination of the device. The device performances are summarized in Fig. 5 and the corresponding data are listed in Table 2.

In accordance with their solid state PL, **TMPDPA** exhibits deepest blue EL, of which wavelength (444 nm) is nearly as short as that of **DPA** (442 nm) and the EL band width (66 nm) is nearly as narrow as that of **DPA** (56 nm). Therefore, 1931 CIE_{x,y} of two OLEDs are comparable deep blue (0.15, 0.05) and (0.17, 0.10) for **DPA** and **TMPDPA**, respectively. EL spectra of **TPSDPA**, **CBZDPA**, and **OXDDPA** are a little red-shifted and broadening, although 1931 CIE_{x,y} chromaticity of these devices remains satisfactory blue colour (all *y*-values are less than 0.20, Table 2). However, EL spectrum of **PPODPA** is significantly worsening and its 1931 CIE_{x,y} (0.22, 0.37) indicates that it is not a blue OLED having unsatisfactory colour purity.



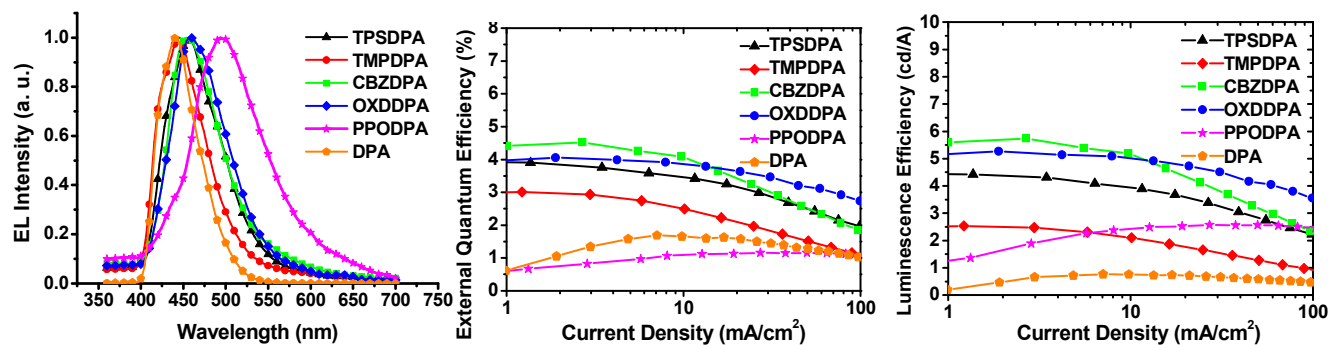


Fig. 5 Electroluminescence characteristics of DPA and DPA derivatives.

Table 2. Characteristics of OLEDs ^[a]

DPA derivatives	Turn-on Voltage (V) ^[b]	Max. Luminance, Voltage (V)	Max. Efficiency (% cd/A, lm/W) ^[c]	λ_{max} EL, fwhm (nm) ^[d]	1931 CIE chromaticity (x, y) ^[d]	Efficiency at 100 and 1000 cd/m ² (% cd/A, lm/W)
DPA	3.5	1134, 15	1.5, 0.7, 0.4	440, 56	(0.15, 0.05)	1.6, 0.8, 0.4; 0.3, 0.7, 0.2
TMPDPA	4.0	1477, 15	3.0, 2.5, 1.9	444, 66	(0.17, 0.10)	2.8, 2.4, 1.5; 1.1, 0.8, 0.3
TPSDPA	3.5	4501, 15	3.8, 4.4, 3.8	458, 76	(0.16, 0.15)	3.7, 4.2, 2.8; 2.9, 3.2, 1.4
PPODPA	4.0	7891, 15	0.7, 2.5, 1.1	496, 96	(0.22, 0.37)	0.6, 1.7, 0.9; 1.1, 2.5, 0.9
CBZDPA	3.5	3377, 15	4.5, 5.7, 3.9	454, 72	(0.17, 0.17)	4.5, 5.6, 3.7; 3.3, 4.0, 1.8
OXDDPA	3.5	6985, 15	4.0, 5.2, 5.1	460, 78	(0.16, 0.18)	4.0, 5.2, 3.6; 3.6, 4.7, 2.3

⁵ [a] ITO/NPB(30 nm)/TCTA(10 nm)/9,10-DPA based derivatives(30 nm)/TPBI(30 nm)/LiF(1 nm)/Al. [b] with electroluminescence at 1 cd/m². [c] at current density of 1 mA/cm². [d] fwhm denotes full-width-at-half-maximum and the EL spectra were recorded at 8.0 V.

For EL efficiency concerns, both **TMPDPA** and **TPSDPA** OLEDs greatly outperform **DPA** OLED with just little compromise of blue color purity. In fact, current density or brightness of **TMPDPA** and **TPSDPA** OLEDs is far more superior compared with that of **DPA** OLED (Figure 5). More specifically, **TPSDPA** OLED is better than **TMPDPA** OLED in EL efficiency, which can be mostly attributed to the higher Φ_f of **TPSDPA** than **TMPDPA** in solid state. Nevertheless, **TMPDPA** OLED is slightly better than **TMPDPA** OLED in blue color purity (1931 CIE_{x,y} in Table 2). For **PPODPA**, OLED performance is much inferior in all aspects, current density, brightness, blue colour purity, and EL efficiency (Figure 5). The unsatisfactory performance of **PPODPA** OLED is mainly due to its poor Φ_f and red-shifted emission in solid state, which can be attributed to its bipolar structure feature that promotes the material crystallization in solid state. **PPODPA** is the one of two DPA derivatives studied herein showing T_c in thermal property measurement (see Fig. 2). Following our previous analysis of spectroscopic data of **PPODPA**, excimer formation is highly possible in the non-dopant device and it explains the low solid state Φ_f (and hence low brightness), low current density (because of charge trapping nature of excimer), and long EL wavelength and hence poor 1931 CIE_{x,y} for blue colour.

From the structural design, **CBZDPA** and **OXDDPA** are considered as two derivatives of **TMPDPA** having charge transporting moiety on the phenyl rings at C-9 and C-10 positions of anthracene core. EL efficiency of **CBZDPA** and **OXDDPA** OLEDs has been drastically improved in comparison with that of **TMPDPA** OLEDs (Fig. 5, Table 2). OLEDs exhibit EL efficiency of 4.5 and 4.0 % at electroluminescence of 100 cd/m², respectively; 3.3 and 3.6% at electroluminescence of 1000 cd/m²,

respectively. **TMPDPA** OLED exhibits EL efficiency only 2.8 and 1.1% at electroluminescence of 100 and 1000 cd/m², respectively. At the first glance, much higher solid state Φ_f of **CBZDPA** and **OXDDPA** than that of **TMPDPA** provides a logical explanation for the acquired EL efficiency of these OLEDs. Furthermore, we think that the charge transport molecular structures of **CBZDPA** and **OXDDPA** also contribute to the enhancement of EL efficiency.

In order to understand the hole and electron transporting nature of **TMPDPA**, **CBZDPA**, and **OXDDPA**, we also fabricated two kinds of single-charge carrier-dominated devices⁷⁰ for exploring the nature of material charge carrier in terms of the current density of such devices. The hole dominated device has a configuration of ITO/NPB(40 nm)/TCTA(10 nm)/DPA derivative(50 nm)/NPB(20 nm)/Al(100 nm). The electron dominated device has a configuration of ITO/BCP(10 nm)/DPA derivative(50 nm)/TPBI(20 nm)/LiF(1 nm)/Al(100 nm). As shown in the inset of Fig. 6, we used high lying LUMO NPB to limit the electron carrier in hole dominated device and low lying HOMO BCP and TPBI to limit the hole carrier in electron dominated device. One should note that the current density of a single-charge carrier-dominated device is determined by several factors, hole injection barrier between the electrode and organic layers, the difference of the HOMO energy levels between adjacent organic layers, and the charge mobility of each organic layers. In the case studied herein, the HOMO energy levels of **TMPDPA** and **CBZDPA** are very similar, which implies the current density of hole dominated device depending on the hole-mobility of the blue emitter solely. The HOMO energy level of **OXDDPA** is about 0.20 to 0.23 eV higher than the other two, which implies the hole carrier should be easier to pass through the device. Considering all factors, the current density of such

device indicates that the hole mobility of three DPA derivatives is descending in **CBADPA** > **TMPDPA** > **OXDDPA** order. The situation of the current density of electron dominated device is quite similar but in a reverse order. The LUMO energy levels of **TMPDPA**, **CBZDPA**, and **OXDDPA** are all lower than the LUMO energy level of TPBI (2.7 eV), which implies there is no

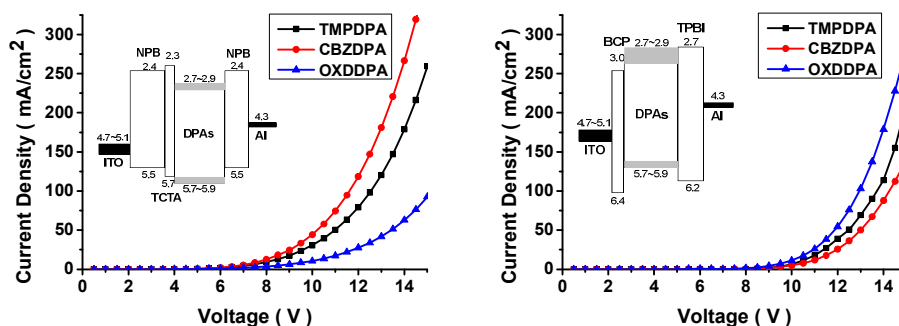


Fig. 6 Current density-voltage (I-V) characteristics of hole dominated device (left) and electron dominated device (right).

Charge transporting nature of light-emitting materials is one of paramount factors in enhancing EL efficiency and reducing efficiency roll-off of the non-dopant OLEDs like ones in present study. Whereas hole transporting nature of **CBZDPA** enhances the EL efficiency at low to medium current density range, electron transporting nature of **OXDDPA** promotes EL efficiency in high current density range. Such difference in current density dependent EL efficiency enhancement results **CBZDPA** the most efficient EL at low current density range but **OXDDPA** becomes the most efficient EL at high current density range (Fig. 5). Efficiency roll-off found more serious in **CBZDPA** OLED than **OXDDPA** OLED is consistent with the inference drawn herein. In addition, from the experimental results of **PPODPA** EL efficiency (Fig. 5, Table 2), there is no efficiency roll-off but “roll-up” at current density as high as 100 mA/cm². Like **OXDDPA**, diphenylphosphine oxide bearing **PPODPA** is bipolar and potential for electron transporting.

Conclusions

In summary, we have synthesized and characterized a series of DPA derivatives, **TPSDPA**, **TMDDPA**, **PPODPA**, **BMTDPA**, **NPADPA**, **CBZDPA**, and **OXDDPA**. Some of these new fluorophores are capable of emitting EL nearly as blue as the EL from **DPA**. All these DPA derivatives are designed with bulky or sterically hindered substituent on C-2 position to prevent the solid state emission from red-shifting and broadening. In addition to one failure **PPODPA** that tends to adversely crystallize to form excimer in condense phase, the emission of **BMTDPA** and **NPADPA** was found seriously quenched and red-shifted due to the electronic reason, i.e., ICT. The non-doped OLEDs fabricated with charge transport bearing **CBZDPA** or **OXDDPA** exhibited the highest external quantum efficiency of 4.5 and 4.0 %, respectively, among all, including **DPA** OLED, which showed only 1.5% with the same device structure. The charge transporting nature of **CBZDPA** and **OXDDPA** has been verified by the current density of hole dominated and electron dominated devices. We have successfully demonstrated that mesityl group on C-2 position are potent in preserving the deep blue fluorescence of **DPA** in solid state. The EL efficiency of **DPA** OLED have been greatly improved by incorporating charge

apparent electron injection barrier at the interface of two layers. The magnitude of current density clearly is decreasing in order of **OXDDPA** > **TMPDPA** > **CBZDPA**, which is accordant with the anticipated order of material electron mobility based on the structure feature of electron deficiency.

transporting moiety on the phenyl rings at C-9 and C-10 positions of anthracene core.

Experimental

General Information

UV-visible electronic absorption spectra were recorded on a Hewlett-Packard 8453 Diode Array Spectrophotometer. Fluorescence spectra were obtained on Hitachi F-5400 fluorescence spectrophotometer with the excitation at 380 nm. The solution fluorescence quantum yields of interesting compounds were determined relative to that of **DPA** in dichloromethane at 298 K ($\Phi_f=0.9$).⁴⁴ The solid-state fluorescence quantum yields (Φ_f) of the blue emitters were determined by the integrating-sphere method.^{71,72} The ionization potentials (or HOMO energy levels) of **DPA** derivatives were determined by low energy photoelectron spectrometer (Riken-Keiki AC-2). LUMO energy levels were estimated by subtracting the energy (ΔE) from HOMO energy levels. ΔE was determined by the on-set absorption energy from the absorption spectra of the thin film materials. The differential scanning calorimetry (DSC) analysis was performed under a nitrogen atmosphere on a Perkin-Elmer DSC-7 differential scanning calorimeter, using a scan rate of 10 °C/min. Thermogravimetric analysis (TGA) was carried out on a Perkin-Elmer DSC-7 thermogravimetric analyzer to determine the decomposition temperatures (T_d) of the compounds under nitrogen atmosphere, using a scan rate of 10 °C/min. ¹H and ¹³C NMR spectra were recorded on Brüker AV-400 or Brüker AV3-400, using deuterated chloroform as the internal standard. High resolution mass spectrometric measurements were obtained on JMS-700 double focusing mass spectrometer (JEOL, Tokyo, Japan) from Mass Spectroscopic Laboratory in-house service of the Institute of Chemistry.

Fabrication and Characterization of Light-Emitting Diodes.

OLED devices were fabricated by thermal vacuum deposition. The substrate was an indium-tin-oxide (ITO) coated glass (Shin An SNP, Taiwan) with a sheet resistance of $\leq 30 \Omega/\text{sq}$. The pretreatment of ITO includes a routine chemical cleaning using detergent, deionized water, acetone and isopropyl alcohol in sequence, followed by oxygen plasma cleaning. The thermal evaporation of organic materials was carried out using CRYOTEC-10 at a chamber pressure of 10^{-6} Torr. The thickness

of each layer was determined by quartz thickness monitor (STM-100/MF and STM-2XM). The cathode of LiF/Al was prepared first thermally deposited a LiF thin film (10 Å) followed by the deposition of Al metal (1000 Å) as the top layer. The thickness of each layer material was determined similarly as before. The devices were all encapsulated with glass slides, which were attached to the device by UV-cured epoxy glue. The effective size of the emitting diode was 4.00 mm², which is significantly smaller than the active area of the photodiode detector, a condition known as “under-filling”, satisfying the measurement protocol.⁷³ This is one of the most conventional ways in measuring the EL efficiency of OLEDs, although sometimes experimental errors may arise due to the non-Lambertian emission of OLEDs.⁷⁴ Current-voltage-luminance (*I-V-L*) measurements were made simultaneously using a Keithley 2400 source meter and a Newport 1835C optical meter equipped with a Newport 818-ST silicon photodiode, respectively. The measurements for devices were made at room temperature under ambient condition. The EL was measured using the fluorescence spectrophotometer (Hitachi F-5400) by blocking the incident light.

Synthesis of Materials

Unless specified condition, all reaction were performed under nitrogen atmosphere using standard Schlenk techniques. All commercially available chemical reagents were used directly without further purification. Compounds like 2-bromo-9,10-diphenylanthracene (**1**),⁷⁵ 2-bromoanthracene (**3**),⁷⁶ 2,4,6-trimethylphenylboronic acid,⁷⁷ 9-(4-(4,4,5,5-tetramethyl-1,3,2-dioxaborolan-2-yl)phenyl)-9*H*-carbazole,⁷⁸ and 2-phenyl-5-(3-(4,4,5,5-tetramethyl-1,3,2-dioxaborolan-2-yl)phenyl)-1,3,4-oxadiazole⁴¹ were prepared according to literatures. For the materials used in device fabrication, BCP (2,9-dimethyl-4,7-diphenyl-1,10-phenanthroline) was commercially available. NPB (4,4'-bis[*N*-(1-naohthyl)-*N*-phenylamino]-buphenyl),⁷⁹ TPBI (2,2',2''-(1,3,5-benzinetriyl)-tris(1-phenyl-1-*H*-benzimidazole)),⁸⁰ and TCTA (tris(4-carbazoyl-9-ylphenyl)amine)⁸¹ were prepared via published methods and were subjected to gradient sublimation prior to use.

9,10-Diphenyl-(2-triphenylsilyl)anthracene (TPSDPA, **2a**)

To a dry diethyl ether solution (60 mL) of 2-bromo-9,10-diphenylanthracene (0.96 g, 2.35 mmol) was added *n*-BuLi (1.66 mL, 4.16 mmol, 2.5 M in hexane) slowly in -78 °C. The mixture was stirred for 45 minutes under nitrogen atmosphere. Chlorotriphenylsilane (1.0 g, 3.39 mmol) in diethyl ether (10 mL) was added dropwise at -78 °C and the mixture was stirred at room temperature for 12 hours. After reaction quenched by water, the mixture was extracted with dichloromethane. The organic layer was dried with magnesium sulphate. After removal of drying agent, the organic solution was evaporated till dryness under reduced pressure. The resulting solid was purified by using column chromatography (silica gel, 10% CH₂Cl₂/hexane) to afford TPSDPA (0.7 g, 44%) as a white solid. ¹H NMR (400 MHz, CDCl₃): δ (ppm): 7.93 (s, 1H), 7.71-7.65 (m, 3H), 7.59-7.45 (m, 13H), 7.38-7.24 (m, 17H). ¹³C NMR (100 MHz, CDCl₃): δ (ppm): 138.96, 138.42, 137.84, 136.82, 136.26, 134.08, 131.34, 131.08, 130.98, 130.52, 130.28, 130.03, 129.92, 129.44, 129.24, 128.37, 128.15, 127.79, 126.92, 125.69, 125.27, 124.93. EI-HRMS: calcd 588.2273, *m/z* = 588.2270 (M⁺).

9,10-Diphenyl-(2-diphenylphosphinyl)anthracene (PPODPA, **2b**)

To a dry THF solution (60 mL) of 2-bromo-9,10-diphenylanthracene (1.0 g, 2.45 mmol) was added *n*-BuLi (1.96 mL, 4.90 mmol, 2.5M in hexane) slowly in -78 °C. The mixture was stirred for 45 minutes under nitrogen atmosphere. Chlorotriphenylphosphine (1.6 mL, 7.1 mmol) was added dropwise at -78 °C and the mixture was stirred at room temperature for 6 hours. After reaction quenched by water, the mixture was extracted with dichloromethane. The separated organic layer was evaporated till dryness under reduced pressure. The residue solid was re-dissolved in CH₂Cl₂ (10 mL) and was treated with H₂O₂ (10 mL, 30 wt% in H₂O) and stirred for another 24 hours. The separated organic layer was dried with magnesium sulphate. After removal of drying agent, the organic solution was evaporated till dryness under reduced pressure. The resulting solid was purified by using column chromatography (silica gel, 10% CH₂Cl₂/EtOAc) to afford PPODPA (0.4 g, 30%) as a light yellow solid. ¹H NMR (400 MHz, CDCl₃): δ (ppm): 7.86-7.28 (d, *J* = 0.8 Hz, 1H), 7.58-7.68 (m, 3H), 7.60-7.33 (m, 22H), 7.29-7.26 (m, 2H). ¹³C NMR (100 MHz CDCl₃): δ (ppm) : 139.08, 138.39, 137.73, 137.29, 134.50, 134.39, 132.73, 132.06, 131.96, 131.75, 131.32, 131.21, 130.98, 130.36, 130.25, 129.35, 128.53, 128.42, 128.35, 128.30, 127.75, 127.58, 127.46, 127.30, 127.03, 126.12, 125.57, 124.97, 124.87. EI-HRMS: calcd 530.1800, *m/z* = 530.1801 (M⁺).

9,10-Diphenyl-(2-dimesitylboranyl)anthracene (BMTDPA, **2c**)

To a dry THF solution (30 mL) of 2-bromo-9,10-diphenylanthracene (0.4 g, 0.98 mmol) was added *n*-BuLi (1.1 mL, 2.84 mmol, 2.5M in hexane) slowly in -78 °C. The mixture was stirred for 45 minutes under nitrogen atmosphere. Dimesitylboron fluoride (0.86 g, 3.23 mmol) in THF (5 mL) was added dropwise at -78 °C and the mixture was stirred at room temperature for 12 hours. After reaction quenched by water, the mixture was extracted with dichloromethane. The organic layer was dried with magnesium sulphate. After removal of drying agent, the organic solution was evaporated till dryness under reduced pressure. The resulting solid was purified by using column chromatography (silica gel, hexane) to afford BMTDPA (0.12 g, 21%) as a yellow-green solid. ¹H NMR (400 MHz, CDCl₃): δ (ppm) : 7.83 (s, 1H), 7.78-7.75 (d, *J* = 8.4 Hz, 1H), 7.71-7.69 (d, *J* = 8Hz, 1H), 7.59-7.47 (m, 6H), 7.42-7.29 (m, 8H), 6.73 (s, 4H), 2.28 (s, 6H), 1.97 (s, 12H). ¹³C NMR (75 MHz, CDCl₃) : δ (ppm): 141.69, 140.48, 140.03, 139.75, 138.87, 138.20, 136.47, 133.90, 131.28, 130.58, 129.65, 129.54, 128.32, 127.92, 127.41, 127.27, 126.91, 125.67, 125.48, 124.86, 123.63, 122.72, 23.42, 21.12. EI-HRMS: calcd 578.3145, *m/z* = 578.3141 (M⁺).

9,10-Diphenyl-(2-phenylnaphthalen-1-amino)anthracene (NPADPA, **2d**)

A mixture of *N*-phenylnaphthalen-1-amine (0.64 g, 2.94 mmol), 2-bromo-9,10-diphenylanthracene (0.8 g, 1.96 mmol), sodium *tert*-butoxide (0.22 g, 2.35mmol), and palladium acetate (0.01 g, 0.05 mmol) in xylene (7 mL) was added tri-*tert*-butylphosphine (0.05 mL, 0.2 mmol) and stirred at 120 °C for 16 hours. After the

reaction was cooled to room temperature, the xylene was removed under reduced pressure. The residue was extracted with dichloromethane and H₂O. The organic layer was dried with magnesium sulphate. After removal of drying agent, the organic solution was evaporated till dryness under reduced pressure. The resulting solid was purified by using column chromatography (silica gel, 10% CH₂Cl₂/hexane) to afford **NPADPA** (0.91 g, 84%) as a yellow solid. ¹H NMR (400 MHz, CDCl₃): δ (ppm): 7.88-7.84 (t, *J* = 8 Hz, 2H), 7.72-7.70 (d, *J* = 8 Hz, 1H), 7.65-7.61 (m, 2H), 7.57-7.54 (t, *J* = 4 Hz, 2H), 7.51-7.45 (m, 4H), 7.43-7.41 (d, *J* = 8 Hz, 1H), 7.37-7.33 (t, *J* = 8 Hz, 1H), 7.29-7.14 (m, 10H), 7.09-7.07 (d, *J* = 8 Hz, 4H), 6.95-6.91 (t, *J* = 8 Hz, 1H), 6.86-6.85 (d, *J* = 12 Hz, 1H). ¹³C NMR (100 MHz, CDCl₃): δ (ppm): 147.65, 144.56, 143.14, 139.09, 138.53, 136.78, 135.23, 131.24, 131.04, 130.80, 130.15, 128.96, 128.29, 127.87, 127.78, 127.35, 127.00, 126.84, 126.65, 126.40, 126.23, 126.07, 125.95, 124.99, 124.17, 124.00, 122.54, 122.46, 122.32, 114.46. EI-HRMS: calcd 547.2300, *m/z* = 547.2292 (M⁺).

2-(1,3,5-Trimethylphenyl)anthracene (4)

A deoxygenated mixture of 2-bromoanthracene (0.18 g, 0.70 mmol), 2,4,6-trimethylphenylboronic acid (0.2 g, 0.77 mmol), K₂CO_{3(aq)} (1.2 mL, 2.31 mmol, 2 M in H₂O), and ethanol (1 mL) in toluene (5 mL) was added tetrakis(triphenylphosphine) palladium(0) (0.04 g, 0.04 mmol) and stirred at 80 °C for 12 hours. After the reaction was cooled to room temperature, the toluene was removed under reduced pressure and the residue was extracted with dichloromethane and H₂O. The organic layer was dried with magnesium sulphate. After removal of drying agent, the organic solution was evaporated till dryness under reduced pressure. The resulting solid was purified by using column chromatography (silica gel, hexane) to afford 2-(1,3,5-trimethylphenyl)anthracene (0.15 g, 55%) as a white solid. ¹H NMR (400 MHz, CDCl₃): δ (ppm): 8.63-8.56 (m, 3H), 8.37 (s, 1H), 7.63-7.60 (m, 2H), 7.45-7.42 (dd, *J* = 1.2 Hz, 1H), 7.00 (s, 2H), 2.36 (s, 3H), 2.06 (s, 6H). ¹³C NMR (125 MHz, CDCl₃): δ (ppm): 138.81, 138.09, 136.71, 136.11, 131.89, 131.69, 130.65, 128.16, 128.05, 127.91, 127.72, 126.03, 125.77, 125.38, 125.23, 21.02, 20.74. FAB-MS: calcd 296.16, *m/z* = 296.2 (M⁺).

9,10-Dibromo-2-(1,3,5-trimethylphenyl)anthracene (5)

To a chloroform solution (2 mL) of 2-(1,3,5-trimethylphenyl)anthracene (0.2 g, 0.67 mmol) and *N*-bromosuccinimide (0.33 g, 1.87 mmol) was stirred at 50 °C for 2 hours under nitrogen atmosphere. After the reaction was cooled to room temperature, the mixture was poured into 2 N NaOH_(aq) and extracted with dichloromethane. The organic layer was dried with magnesium sulphate. After removal of drying agent, the organic solution was evaporated till dryness under reduced pressure. The residue was purified by using column chromatography (silica gel, hexane) to afford 9,10-dibromo-2-(1,3,5-trimethylphenyl)anthracene (0.2 g, 65%) as a yellow solid. ¹H NMR (400 MHz, CDCl₃): δ (ppm): 8.63-8.56 (m, 3H), 8.37 (s, 1H), 7.63-7.60 (m, 2H), 7.45-7.42 (dd, *J* = 1.2 Hz, 1H), 7.00 (s, 2H), 2.36 (s, 3H), 2.06 (s, 6H). ¹³C NMR (125 MHz, CDCl₃): δ (ppm): 140.36, 137.94, 137.17, 135.95, 131.26, 130.98, 130.10, 129.98, 129.75, 128.44, 128.30, 128.24, 128.19, 128.05, 127.45, 127.30, 123.4, 123.33, 21.00, 20.78. MALDI-MS: calcd 451.98, *m/z* = 451.9 (M⁺).

9,10-Bis(4-carbazole)phenylene-2-(1,3,5-trimethylphenyl)anthracene (CBZDPA, 6a)

This compound was prepared similarly to that of 9,10-diphenyl-2-(1,3,5-trimethylphenyl)anthracene, except that 9-(4-(4,4,5,5-tetramethyl-1,3,2-dioxaborolan-2-yl)phenyl)-9*H*-carbazole (0.37 g, 0.99 mmol), two drops of Aliquat 336 and triphenylphosphine (0.034 g, 0.13 mmol) were added in the reaction and the reaction continued for 24 hours. A mixed solvent of 15% EtOAc/hexane was used as eluent for column chromatography. **CBZDPA** was obtained as a white solid (0.15 g, 60%). ¹H NMR (400 MHz, CDCl₃): δ (ppm): 8.21-8.17 (m, 4H), 7.94-7.85 (m, 4H), 7.74-7.66 (m, 7H), 7.53-7.46 (m, 6H), 7.38-7.29 (m, 5H), 6.97 (s, 1H), 2.32 (s, 3H), 2.09 (s, 6H). ¹³C NMR (100 MHz, CDCl₃): δ (ppm): 140.91, 140.77, 138.77, 138.16, 138.02, 137.88, 137.22, 136.91, 136.36, 136.16, 132.86, 132.74, 130.45, 130.04, 129.00, 128.33, 128.18, 127.66, 127.43, 127.00, 126.88, 126.82, 126.73, 126.05, 125.98, 125.55, 125.39, 123.58, 120.42, 120.33, 120.14, 120.10, 110.10, 109.95, 20.99, 20.96. EI-HRMS: calcd 778.3348, *m/z* = 778.3329 (M⁺).

9,10-Diphenyl-2-(1,3,5-trimethylphenyl)anthracene (TMPDPA, 6b)

A deoxygenated mixture of 9,10-dibromo-2-(1,3,5-trimethylphenyl)anthracene (0.2 g, 0.44 mmol), phenylboronic acid (0.13 g, 1.1 mmol), K₂CO_{3(aq)} (1.2 mL, 2.31 mmol, 2 M in H₂O), and ethanol (0.5 mL) in toluene (2.2 mL) was added tetrakis(triphenylphosphine)palladium (0.04 g, 0.04 mmol) and stirred at 80 °C for 12 hours. After cooling to room temperature, the toluene solvent was removed under reduced pressure and the residue was extracted with dichloromethane and water. The organic layer was dried with magnesium sulphate. After removal of drying agent, the organic solution was evaporated till dryness under reduced pressure. The resulting solid was purified by using column chromatography (silica gel, 10% dichloromethane/hexane) to afford **TMPDPA** (0.1 g, 50%) as a white solid. ¹H NMR (400 MHz, CDCl₃): δ (ppm): 7.74-7.59 (m, 6H), 7.56-7.44 (m, 10H), 7.32-7.30 (m, 2H), 7.15-7.12 (dd, *J* = 4 Hz, 1H), 6.90 (s, 2H), 2.29 (s, 3H), 1.99 (s, 6H). ¹³C NMR (100 MHz, CDCl₃): δ (ppm): 139.14, 137.35, 137.00, 136.65, 136.14, 133.57, 133.07, 132.17, 131.38, 131.26, 130.16, 129.97, 129.86, 128.86, 128.41, 128.14, 127.57, 127.46, 126.91, 126.09, 125.00, 124.88, 123.38. EI-HRMS: calcd 448.2191, *m/z* = 448.2197 (M⁺).

9,10-Bis[3-(3-phenyl-2,4,5-oxadiazole)phenylene]-2-(1,3,5-trimethylphenyl)anthracene (OXDDPA, 6c)

This compound was prepared similarly to that of **TMPDPA**, except 2-phenyl-5-(3-(4,4,5,5-tetramethyl-1,3,2-dioxaborolan-2-yl)phenyl)-1,3,4-oxadiazole (1.91 g, 5.5 mmol) used in the reaction. In addition, a mixed solvent of 20% EtOAc/hexane was used as eluent for column chromatography. **OXDDPA** was obtained as a white solid (1.2 g, 74%). ¹H NMR (400 MHz, CDCl₃): δ (ppm): 8.41-8.38 (m, 1H), 8.31-8.30 (s, *J* = 4 Hz, 2H), 8.25 (s, 1H), 8.12-8.08 (t, *J* = 8 Hz, 4H), 7.84-7.80 (dt, *J* = 8 Hz, 1H), 7.76-7.66 (m, 6H), 7.52-7.47 (m, 7H), 7.39-7.36 (m, 2H), 7.23-7.19 (d, *J* = 4 Hz, 1H), 6.89-6.86 (d, *J* = 12 Hz, 2H), 2.25 (s, 3H), 2.00 (s, 6H). ¹³C NMR (100 MHz, CDCl₃): δ (ppm): 164.70, 164.47, 140.13, 140.01, 138.46, 138.09, 136.85, 135.97,

135.85, 134.59, 134.53, 131.70, 130.01, 129.87, 129.76, 129.53, 129.43, 129.01, 128.81, 128.21, 126.91, 126.63, 126.46, 126.28, 125.64, 125.52, 124.46, 123.85, 20.82. EI-HRMS: calcd 736.2838, $m/z = 736.2845$ (M^+).

5 Acknowledgement

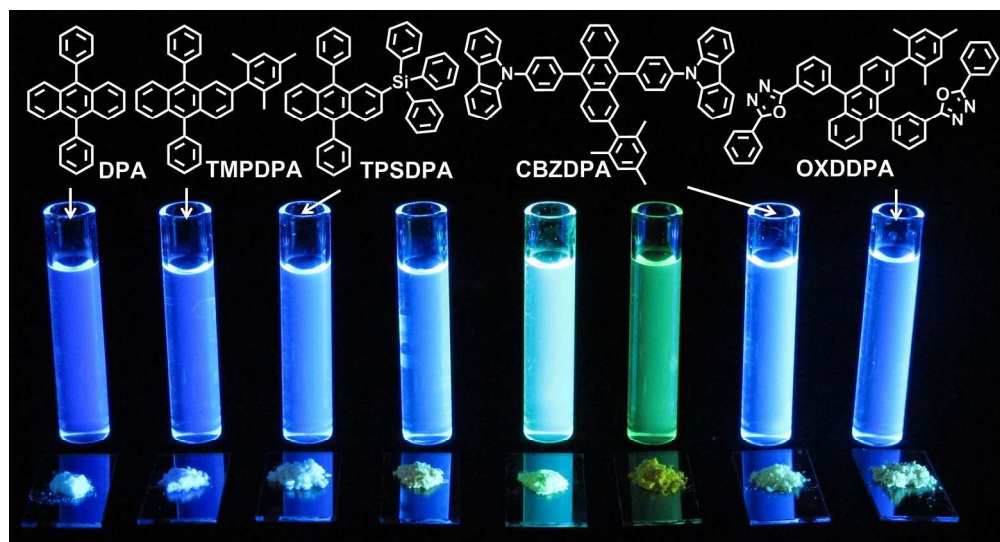
This work was partially supported by National Science Council (NSC 101-2113-M-001 -004 -MY2), Academia Sinica, and National Taiwan University. Supporting personnel from Chung Shan Medical University is acknowledged.

10 References

1. L. Xiao, Z. Chen, B. Qu, J. Luo, S. Kong, Q. Gong and J. Kido, *Adv. Mater.*, 2011, **23**, 926.
2. Y. Chi and P.-T. Chou, *Chem. Soc. Rev.*, 2010, **39**, 638.
3. H. Fu, Y.-M. Cheng, P.-T. Chou and Y. Chi, *Materials Today*, 2011, **14**, 472.
4. C.-H. Yang, M. Mauro, F. Polo, S. Watanabe, I. Muenster, R. Fröhlich and L. D. Cola, *Chem. Mater.*, 2012, **24**, 3684
5. F. Kessler, Y. Watanabe, H. Sasabe, H. Katagiri, Md. K. Nazeeruddin, M. Grätzel and J. Kido, *J. Mater. Chem. C*, 2013, **1**, 1070
6. Y. Sun, N. C. Giebink, H. Kanno, B. Ma, M. E. Thompson and S. R. Forrest, *Nature*, 2006, **440**, 908.
7. G. Schwartz, S. Reineke, T. C. Rosenow, K. Walzer and K. Leo, *Adv. Funct. Mater.*, 2009, **19**, 1319.
8. M. E. Kondakova, J. C. Deaton, T. D. Pawlik, D. J. Giesen, D. Y. Kondakova, R. H. Young, T. L. Royster, D. L. Comfort and J. D. Shore, *J. Appl. Phys.*, 2010, **107**, 014515
9. J. Ye, C. J. Zheng, X. M. Ou, X. H. Zhang, M. K. Fung and C. S. Lee, *Adv. Mater.*, 2012, **24**, 3410.
10. C. Adachi, T. Tsutsui and S. Saito, *Appl. Phys. Lett.*, 1990, **56**, 799.
11. Y. H. Kim, D. C. Shin, S. H. Kim, C. H. Ko, H. S. Yu, Y. S. Chae and S. K. Kwon, *Adv. Mater.*, 2001, **13**, 1690.
12. K. Danel, T.-H. Huang, J. T. Lin, Y.-T. Tao and C.-H. Chuen, *Chem. Mater.*, 2002, **14**, 3860.
13. B. Balaganesan, W.-J. Shen and C. H. Chen, *Tetrahedron Lett.*, 2003, **44**, 5747.
14. M.-T. Lee, H.-H. Chen, C.-H. Liao, C.-H. Tsai and C. H. Chen, *Appl. Phys. Lett.*, 2004, **85**, 3301.
15. W.-J. Shen, R. Dodda, C.-C. Wu, F.-I. Wu, T.-H. Liu, H.-H. Chen, C. H. Chen and C.-F. Shu, *Chem. Mater.*, 2004, **16**, 930.
16. M.-T. Lee, H.-H. Chen, C.-H. Liao, C.-H. Tsai and C. H. Chen, *Adv. Mater.*, 2005, **17**, 2493.
17. Y.-H. Kim, H.-C. Jeong, S.-H. Kim, K. Yang and S.-K. Kwon, *Adv. Funct. Mater.*, 2005, **15**, 1799.
18. M.-H. Ho, Y.-S. Wu, S.-W. Wen, M.-T. Lee, T.-M. Chen, C. H. Chen, K.-C. Kwok, S.-K. So, K.-T. Yeung, Y.-K. Cheng and Z.-Q. Gao, *Appl. Phys. Lett.*, 2006, **89**, 252903.
19. P.-I. Shih, C.-Y. Chuang, C.-H. Chien, E. W.-G. Diao and C.-F. Shu, *Adv. Funct. Mater.*, 2007, **17**, 3141.
20. S.-K. Kim, Y.-I. Park, I.-N. Kang and J.-W. Park, *J. Mater. Chem.*, 2007, **17**, 4670.
21. Y.-Y. Lyu, J. Kwak, O. Kwon, S.-H. Lee, D. Kim, C. Lee and K. Char, *Adv. Mater.*, 2008, **20**, 2720.
22. Y.-I. Park, J.-H. Son, J.-S. Kang, S.-K. Kim, J.-H. Lee and J.-W. Park, *Chem. Commun.*, 2008, 2143.
23. S.-K. Kim, B. Yang, Y. Ma, J.-Y. Lee and J. Park, *J. Mater. Chem.*, 2008, **18**, 3376.
24. L. Wang, W.-Y. Wong, M.-F. Lin, W.-K. Wong, K.-W. Cheah, H.-L. Tam and C. H. Chen, *J. Mater. Chem.*, 2008, **18**, 4529.
25. S. Tao, Y. Zhou, C.-S. Lee, S.-T. Lee, D. Huang and X. Zhang, *J. Phys. Chem. C*, 2008, **112**, 14603.
26. C.-H. Chien, C.-K. Chen, F.-M. Hsu, C.-F. Shu, P.-T. Chou and C.-H. Lai, *Adv. Funct. Mater.*, 2009, **19**, 560.
27. M.-H. Ho, M.-T. Hsieh, K.-H. Lin, T.-M. Chen, J.-F. Chen and C. H. Chen, *Appl. Phys. Lett.*, 2009, **94**, 023306.
28. B. Balaganesan, W.-J. Shen and C. H. Chen, *Tetrahedron Lett.*, 2003, **44**, 5747.
29. C.-H. Wu, C.-H. Chien, F.-M. Hsu, P.-I. Shih and C.-F. Shu, *J. Mater. Chem.*, 2009, **19**, 1464.
30. M. A. Reddy, A. Thomas, K. Srinivas, V. J. Rao, K. Bhanuprakash, B. Sridhar, A. Kumar, M. N. Kamalasanan and R. Srivastava, *J. Mater. Chem.*, 2009, **19**, 6172.
31. C.-J. Zheng, W.-M. Zhao, Z.-Q. Wang, D. Wang, J. Ye, X.-M. Ou, X.-H. Zhang, C.-S. Lee and S.-T. Lee, *J. Mater. Chem.*, 2010, **20**, 1560.
32. S. Ye, J. Chen, C. Di, Y. Liu, K. Lu, W. Wu, C. Du, Y. Liu, Z. Shuai and G. Yu, *J. Mater. Chem.*, 2010, **20**, 3186.
33. Z.-Y. Xia, Z.-Y. Zhang, J.-H. Su, Q. Zhang, K.-M. Fung, M.-K. Lam, K.-F. Li, W.-Y. Wong, K.-W. Cheah, H. Tan and C. H. Chen, *J. Mater. Chem.*, 2010, **20**, 3768.
34. Z. Y. Xia, J.-H. Su, W.-Y. Wong, K.-W. Cheah, H. Tian and C. H. Chen, *J. Mater. Chem.*, 2010, **20**, 8382.
35. M.-S. Gong, H.-S. Lee and Y.-M. Jeon, *J. Mater. Chem.*, 2010, **20**, 10735.
36. J. Huang, B. Xu, J.-H. Su, C. H. Chen and H. Tian, *Tetrahedron*, 2010, **66**, 7577.
37. Y. Sun, L. Duan, D. Zhang, J. Qiao, G. Dong, L. Wang and Y. Qiu, *Adv. Funct. Mater.*, 2011, **21**, 1881.
38. A. Thangthong, D. Meunmart, N. Prachumrak, S. Jungsuttiwong, T. Keawin, E. Sudyoadsuk and V. Promarak, *Chem. Commun.*, 2011, **47**, 7122.
39. K.-R. Wee, W.-S. Han, J.-E. Kim, A.-L. Kim, S. Kwon and S. O. Kang, *J. Mater. Chem.*, 2011, **21**, 1115.
40. J. Huang, J.-H. Su, X. Li, M.-K. Lam, K.-M. Fuang, H.-H. Fan, K.-W. Cheah, C. H. Chen and H. Tian, *J. Mater. Chem.*, 2011, **21**, 2957.
41. M. Zhu, Q. Wang, Y. Gu, X. Cao, C. Zhong, D. Ma, J. Qin and C. Yang, *J. Mater. Chem.*, 2011, **21**, 6409.
42. S.-H. Lin, F.-I. Wu, H.-Y. Tsai, P.-Y. Chou, H.-H. Chou, C.-H. Cheng and R.-S. Liu, *J. Mater. Chem.*, 2011, **21**, 8122.
43. S. H. Kim, I. Cho, M. K. Sim, S. Park and S. Y. Park, *J. Mater. Chem.*, 2011, **21**, 9139.
44. K. H. Lee, J. K. Park, J. H. Seo, S. W. Park, Y. S. Kim, Y. K. Kim and S. S. Yoon, *J. Mater. Chem.*, 2011, **21**, 13640.
45. J. C. Ribierre, A. Ruseckas, H. Cavaye, H. S. Barcena, P. L. Burn and I. D. W. Samuel, *J. Phys. Chem. A*, 2011, **115**, 7401.
46. M. Zhu, T. Ye, C.-G. Li, X. Cao, C. Zhong, D. Ma, J. Qin and C. Yang, *J. Phys. Chem. C*, 2011, **115**, 17965.
47. L. Wang, Z.-Y. Wu, W.-Y. Wong, K.-W. Cheah, H. Huang and C. H. Chen, *Org. Electron.*, 2011, **12**, 595.
48. M.-G. Shin, S. O. Kim, H. T. Park, S. J. Park, H. S. Yu, Y.-H. Kim and S.-K. Kwon, *Dyes Pigm.*, 2012, **92**, 1075.
49. I. Cho, S. H. Kim, J. H. Kim, S. Park and S. Y. Park, *J. Mater. Chem.*, 2012, **22**, 123.
50. H. Park, J. Lee, I. Kang, H. Y. Chu, J.-I. Lee, S.-K. Kwon and Y.-H. Kim, *J. Mater. Chem.*, 2012, **22**, 2695.
51. Z.-Q. Wang, C. Xu, W.-Z. Wang, L.-M. Duan, Z. Li, B.-T. Zhao and B.-M. Ji, *New J. Chem.*, 2012, **36**, 662.
52. H. Fukagawa, T. Shimizu, N. Ohbe, S. Tokito, K. Tokumaru and H. Fujikake, *Org. Electron.*, 2012, **13**, 1197.
53. M.-Y. Teng, Q.-L. Xu, H.-Y. Li, L. Wu, Y.-X. Zheng, C. Lin and L. Wang, *RSC Adv.*, 2012, **2**, 10175.
54. J. Huang, J.-H. Su and H. Tian, *J. Mater. Chem.*, 2012, **22**, 10977.
55. R. Kim, S. Lee, K.-H. Kim, Y.-J. Lee, S.-K. Kwon, J.-J. Kim and Y.-H. Kim, *Chem. Commun.*, 2013, **49**, 4664.
56. J.-A. Seo, C.-W. Lee, M.-S. Gong, *Dyes Pigm.*, 2013, **96**, 211.
57. W. Wan, H. Du, J. Wang, Y. Le, H. Jiang, H. Chen, S. Zhu, and J. Hao, *Dyes Pigm.*, 2013, **96**, 642.
58. N. Prachumrak, S. Namuangruk, T. Keawin, S. Jungsuttiwong, T. Sudyoadsuk and V. Promarak, *Eur. J. Org. Chem.*, 2013, 3825.
59. P. Zhang, W. Dou, Z. Ju, L. Yang, X. Tang, W. Liu and Y. Wu, *Org. Electron.*, 2013, **14**, 915.
60. Y.-C. Chang, S.-C. Yeh, Y.-H. Chen, C.-T. Chen, R.-H. Lee and R.-J. Jeng, *Dyes Pigm.*, 2013, **99**, 577.
61. Y.-Y. Chien, K.-T. Wong, P.-T. Chou and Y.-M. Cheng, *Chem. Commun.*, 2002, 2874.
62. K.-T. Wong, S.-Y. Ku, Y.-M. Cheng, X.-Y. Lin, Y.-Y. Hung, S.-C. Pu, P.-T. Chou, G.-H. Lee and S.-M. Peng, *J. Org. Chem.*, 2006, **71**, 456.
63. Y.-H. Lin, H.-H. Wu, K.-T. Wong, C.-C. Hsieh, Y.-C. Lin, P.-T. Chou, *Org. Lett.*, 2008, **10**, 3211.
64. W. Wu, S. Ye, L. Huang, L. Xiao, Y. Fu, Q. Huang, G. Yu, Y. Liu, J. Qin, Q. Li and Z. Li, *J. Mater. Chem.*, 2012, **22**, 6374.

65. J. Huang, Y. Jiang, J. Yang, R. Tang, N. Xie, Q. Li, H. S. Kwok, B. Z. Tang and Z. Li, *J. Mater. Chem. C* 2014, **2**, 2028.
66. J. Huang, N. Sun, P. Chen, R. Tang, Q. Li, D. Ma and Z. Li, *Chem. Commun.* 2014, **50**, 2136.
- 5 67. A. D. Becke, *J. Chem. Phys.*, 1993, **98**, 5648.
68. M. E. Casida, In *Recent Advances in Density Functional Methods, Part 1*; D. P. Chong, Ed.; World Scientific: Singapore, 1995; p 155.
69. J. Kong, C. A. White, A. I. Krylov, C. D. Sherrill, R. D. Adamson, T. R. Furlani, M. S. Lee, A. M. Lee, S. R. Gwaltney, T. R. Adams, C.
- 10 Ochsenfeld, A. T. B. Gilbert, G. S. Kedziora, V. A. Rassolov, D. R. Maurice, N. Nair, Y. Shao, N. A. Besley, P. E. Maslen, J. P. Dombroski, H. Daschel, W. Zhang, P. P. Korambath, J. Baker, E. F. C. Byrd, T. Van Voorhis, M. Oumi, S. Hirata, C.-P. Hsu, N. Ishikawa, J. Florian, A. Warshel, B. G. Johnson, P. M. W. Gill, M. Head-Gordon and J. A. Pople,
- 15 *J. Comput. Chem.*, 2000, **21**, 1532.
70. C.-C. Chi, C.-L. Chiang, S.-W. Liu, H. Yueh, C.-T. Chen and C.-T. Chen, *J. Mater. Chem.*, 2009, **19**, 5561.
71. J. C de Mello, H. F. Wittmann and R. H. Friend, *Adv. Mater.*, 1997, **9**, 230.
- 20 72. C.-L. Chiang, M.-F. Wu, D.-C. Dai, Y.-S. Wen, J.-K. Wang and C.-T. Chen, *Adv. Funt. Mater.*, 2005, **15**, 231.
73. S. R. Forrest, D. D. C. Bradley and M. E. Thompson, *Adv. Mater.*, 2003, **15**, 1043.
74. I. Tanaka and S. Tokito, *Jpn. J. Appl. Phys.*, 2004, **43**, 7733.
- 25 75. H. Nomura, S. Kawakami, N. Ohsawa and T. Suzuki, *U.S. Patent* 2009/0004506.
76. R. S. Coleman and M. A. Mortensen, *Tetrahedron Lett.*, 2003, **44**, 1215.
77. R. Wipf and J.-K. Jung, *J. Org. Chem.*, 2000, **65**, 6319.
- 30 78. Y.-H. Sun, X.-H. Zhu, Z. Chen, Y. Zhang and Y. Cao, *J. Org. Chem.*, 2006, **71**, 6281.
79. T. Yamamoto, M. Nishiyama and Y. Koie, *Tetrahedron Lett.*, 1998, **39**, 2367.
80. A. J. Canty, N. J. Minchin, L. M. Engelhardt, B. W. Skelton and A. H.
- 35 White, *Aust. J. Chem.*, 1988, **41**, 651.
81. M. Watanabe, M. Nishiyama, T. Yamamoto, Y. Koie, *Tetrahedron Lett.*, 2000, **41**, 481.

Charge transport bearing 9,10-diphenylanthracene derivatives for true blue and efficiency enhancing electroluminescence.



381x204mm (150 x 150 DPI)